Published online 16 October 2022 *Nucleic Acids Research, 2022, Vol. 50, No. 19* ***11093–11108***
https://doi.org/10.1093/nar/gkac823

USP15 promotes cGAS activation through deubiquitylation and liquid condensation

Chengrui Shi[1,2,3,†], Xikang Yang[1,2,3,†], Yanfei Hou[1,2], Xue Jin[4], Lerui Guo[1,2,3], Yi Zhou[1,2,3], Conggang Zhang[1,2] and Hang Yin[1,2,3,*]

[1]School of Pharmaceutical Sciences, Key Laboratory of Bioorganic Phosphorus Chemistry and Chemical Biology (Ministry of Education), Tsinghua University, Beijing 100082, China, [2]Tsinghua University-Peking University Joint Center for Life Sciences, Tsinghua University, Beijing 100084, China, [3]Beijing Advanced Innovation Center for Structural Biology, Tsinghua University, Beijing 100082, China and [4]Peking University–Tsinghua University–National Institute of Biological Science (PTN) Joint Graduate Program, Academy for Advanced Interdisciplinary Studies, Peking University, Beijing 100871, China

Received April 23, 2022; Revised September 08, 2022; Editorial Decision September 09, 2022; Accepted September 14, 2022

ABSTRACT

Double-stranded DNA (dsDNA) is recognized as a danger signal by cyclic GMP-AMP synthase (cGAS), which triggers innate immune responses. cGAS activity must be properly regulated to maintain immune homeostasis. However, the mechanism by which cGAS activation is controlled remains to be better understood. In this study, we identified USP15 as a cGAS-interacting partner. USP15 promoted DNA-induced cGAS activation and downstream innate immune responses through a positive feedback mechanism. Specifically, USP15 deubiquitylated cGAS and promoted its activation. In the absence of DNA, USP15 drove cGAS dimerization and liquid condensation through the USP15 intrinsic disordered region (IDR), which prepared cGAS for a rapid response to DNA. Upon DNA stimulation, USP15 was induced to express and boost cGAS activation, functioning as an efficient amplifier in innate immune signal transduction. In summary, the positive role played by USP15-mediated cGAS activation may be a novel regulatory mechanism in the fine-tuning of innate immunity.

INTRODUCTION

As a pattern recognition receptor (PRR), cyclic GMP-AMP synthase (cGAS) recognizes double-stranded DNA (dsDNA) and plays essential roles in innate immunity (1). Upon DNA binding, cGAS becomes enzymatically active and produces cyclic GMP-AMP (cGAMP), a second messenger that binds the stimulator of the interferon (IFN) gene (STING, also known as TMEM173), leading to conformational changes that trigger oligomerization and activation (2–5). After trafficking from the endoplasmic reticulum (ER) to the Golgi, activated STING recruits TANK-binding kinase 1 (TBK1) to promote TBK1 autophosphorylation, STING phosphorylation at Ser366 and subsequent recruitment and phosphorylation of interferon regulatory factor 3 (IRF3) (6–8). Phosphorylated dimeric IRF3 then is translocated into the nucleus where it induces the expression of type I IFNs and several other inflammatory cytokines and chemokines (9).

cGAS senses DNA from invading pathogens and triggers host immune defenses. However, cGAS can be activated by self-DNA from the cell lysate or cancer cells, and then warns cells to respond to the danger immediately. Thus, cGAS plays important roles in host defense and tumor immunity. However, cGAS can also be overactivated by aberrantly accumulated DNA and cause autoimmune diseases. Therefore, the cGAS–STING pathway must be finely regulated to maintain the immunological balance. A multitude of physiological regulatory mechanisms of cGAS have been illustrated, including ubiquitination. Ubiquitination regulates cGAS stability, promoting its DNA binding availability and enzymatic activity. cGAS can be ubiquitinated by several E3 ligases, but only K48-linked deubiquitylases (DUBs) have been identified (10,11). Elaborate studies have shown the mechanism of cGAS activation by dsDNA, and it is generally believed that cGAS undergoes phase separation after DNA binding. Therefore, changes to the phase separation process can also regulate cGAS activation, but few works have focused on this process (12–14). The primary mechanism of cGAS activation is binding with dsDNA, and recent works have shown that cGAS can also be independently activated by Mn^{2+} ions (15,16). Whether other mechanisms cause cGAS activation remains to be further explored.

*To whom correspondence should be addressed. Tel: +86 1062786005; Fax: +86 1062786005; Email: yin_hang@tsinghua.edu.cn
†The authors wish it to be known that, in their opinion, the first two authors should be regarded as Joint First Authors.

USP15 is a member of the subfamily of cysteine protease DUBs, which catalytically remove the ubiquitin from substrates in a ubiquitin-directed manner. USP15-mediated deubiquitylation has been reported to play multiple roles in regulating innate immune responses. For example, several groups have reported that USP15 positively regulated RIG-I-mediated antiviral signaling by deubiquitylating and stabilizing TRIM25, an important E3 ligase that activates RIG-I by promoting its K63-linked ubiquitination (17–19). In contrast, two other groups reported that USP15 inhibited virus-induced type I IFN production by directly deubiquitylating RIG-I or TBK1 (20,21). Therefore, the role of USP15 in antiviral innate immunity remains to be further clarified. Furthermore, the specific function of USP15 in the DNA-sensing pathway remains unknown.

In this study, we found that USP15 is a cGAS-interacting protein. USP15 expression was induced by DNA-mediated cGAS activation. In human and mouse cells, USP15 promoted cGAS activation through a positive feedback loop. Mechanistically, USP15 deubiquitylated cGAS and promoted its activation. Moreover, USP15 drove cGAS dimerization and liquid condensation, and prepared it to respond rapidly to DNA stimulation in the absence of stimuli. In response to DNA stimuli, the expression of USP15 was induced, which promoted cGAS dimerization and phase separation through the USP15 intrinsic disordered region (IDR). Therefore, in contrast to other traditional cGAS deubiquitylation mechanisms (e.g. USP14-mediated cGAS deubiquitylation) (11), USP15 functions through two parallel routes (mediating cGAS deubiquitylation and promoting its phase separation) to activate cGAS in the presence of DNA. Taken together, our findings elucidate a previously unknown mechanism of cGAS regulation, which may imply a new strategy for therapeutic biotechnology development.

MATERIALS AND METHODS

The materials used are listed in Supplementary Table S1.

Cell lines

Human embryonic kidney (HEK)293T, HeLa, RAW264.7, L929, Vero cells, mouse embryonic fibroblasts (MEFs) and bone marrow-derived macrophages (BMDMs) were cultured in Dulbecco's modified Eagle's medium (DMEM) (Gibco) supplemented with 10% (v/v) fetal bovine serum (FBS), 2 mM L-glutamine, 100 U/ml penicillin and 100 mg/ml streptomycin. THP-1 cells were cultured in RPMI 1640 medium (Gibco) supplemented with 10% (v/v) FBS, 2 mM L-glutamine, 100 U/ml penicillin and 100 mg/ml streptomycin. BMDMs were isolated from mouse femurs and tibias, and cultured with macrophage colony-stimulating factor (M-CSF; 20 ng/ml) to induce differentiation before use. All cultured cells were grown at 37°C in a humidified incubator containing 5% CO_2. All cell lines tested negative for mycoplasma contamination.

Plasmid construction

All the expression plasmids were constructed in existing vectors through homologous recombination with pre-existing vectors using a pEASY-Uni Seamless Cloning and Assembly Kit (TransGen). Point mutations were achieved by using the Fast Mutagenesis System (TransGen). cDNA was obtained by standard polymerase chain reaction (PCR) techniques. The accuracy of all constructs was confirmed by sequencing.

Protein expression and purification

Human cGAS or USP15 was cloned into a pGEX6p-1 plasmid or pET28b plasmid to express glutathione *S*-transferase (GST)-tagged or His6-SUMO-tagged proteins. All recombinant proteins were purified from *Escherichia coli*. The BL21 (DE3) *E. coli* strain harboring GST- or His6-SUMO-tagged proteins was induced with 0.5 mM isopropyl-β-D-thiogalactopyranoside (IPTG) at 18°C for 20 h.

For His6-SUMO-tagged cGAS or His6-tagged USP15 expression, bacteria were sonicated in lysis buffer containing 20 mM Tris, pH 7.5, 500 mM NaCl, 25 mM imidazole, 5 mM β-mercaptoethanol and 0.2 mM phenylmethylsulfonyl fluoride (PMSF). After centrifugation at 12 000 rpm for 60 min, the supernatant was incubated with Ni-NTA beads (GE Healthcare), washed with lysis buffer and eluted with 20 mM Tris, pH 7.5, 500 mM NaCl and 250 mM imidazole. For cGAS purification, after SUMO protease (Ulp1) digestion overnight at 4°C, untagged cGAS was purified on a HiTrap heparin column (GE Healthcare) with a gradient of 0.5–1 M NaCl in 20 mM Tris–HCl, pH 7.5. All proteins were followed by size-exclusion chromatography using a buffer of 20 mM Tris–HCl, pH 7.5, 300 mM NaCl on a Superdex200 10/300 column (GE Healthcare). Fractions were analyzed by sodium dodecylsulfate–polyacrylamide gel electrophoresis (SDS–PAGE), and relevant fractions were combined and concentrated for further use.

For GST-tagged protein expression, bacteria were sonicated in a lysis buffer of 20 mM Tris, pH 7.5, 500 mM NaCl, 5 mM β-mercaptoethanol and 0.2 mM PMSF. After centrifugation at 12 000 rpm for 60 min, the supernatant was incubated with glutathione beads (GE Healthcare), washed with lysis buffer and eluted with 20 mM Tris, pH 7.5, 500 mM NaCl and 50 mM GSH. Proteins were analyzed by SDS–PAGE.

GST pull-down assay

Recombinant GST–cGAS or GST–USP15 proteins (2 μg) were mixed in IP lysis buffer (50 mM Tris–HCl, pH 7.5, 150 mM NaCl, 0.2% Triton X-100 and 10% glycerol) and incubated with glutathione beads (GE Healthcare) at 4°C for 2 h. Protein-bound beads were washed three times with the IP wash buffer (50 mM Tris–HCl, pH 7.5, 300 mM NaCl, 0.2% Triton X-100 and 10% glycerol). Proteins were eluted from the beads by boiling in SDS–PAGE loading buffer and analyzed by Coomassie blue staining.

DNA pull-down assay

Cells seeded in 6-well plates were collected and lysed with IP lysis buffer (with protease inhibitor cocktail). Debris was removed by centrifugation, and 60 μl of supernatant was

kept as the whole-cell lysate. A 5 μg aliquot of biotin–IFN-stimulatory DNA (ISD) or DNA (100 bp) was added to the remaining supernatants (label-free ISD or DNA was used as the control) and incubated at 4°C for 4 h, followed by the addition of streptavidin–Sepharose beads and incubation for 2 h. Beads bound with proteins were washed three times with IP lysis buffer (300 mM NaCl), resuspended in SDS–PAGE loading buffer, denatured and analyzed by immunoblotting.

Generation of stably overexpressing and knockout (KO) cell lines

PTY lentiviral overexpression plasmids or LentiCRISPR-V2 plasmids were constructed to generate stably overexpressing or KO cell lines. HEK293T cells were plated in 10 cm dishes and transfected with lentiviral overexpression or plasmid (8 μg) together with the packaging plasmids psPAX2 (6 μg) and pMD2.G (2 μg). Cell culture medium containing lentiviral particles was harvested 24 h and 48 h after transduction, filtered through a 0.45 μm membrane filter and used to infect the indicated target cells in the presence of 8 μg/ml polybrene. After 48 h of culture, transduced cells were selected with puromycin. The sequences of the guide RNA (gRNA) were as follows: Usp15-g1, GGCGGATCTGGACACCCAGCGG; Usp15-g2, GAACCAGCGACTATCGACTAGG; Cgas-g1, GTTCGGCCCCGCCAGGAAGTCGG; and Cgas-g2, GGCCCCCATTCTCGTACGGAGGG.

Immunoprecipitation (IP)

Cells were lysed in IP lysis buffer (50 mM Tris–HCl, pH 7.5, 150 mM NaCl, 0.2% Triton X-100 and 10% glycerol) supplemented with protease inhibitor cocktail. Debris was removed by centrifugation at 13 000 rpm for 10 min. A 60 μl aliquot of supernatant was retained as the whole-cell lysate, and the remainder was incubated with a specific antibody (or an equal amount of IgG as a control) at 4°C for 2 h, followed by the addition of protein A/G agarose (Santa Cruz) and incubation overnight. For IP with Flag-M2 or Myc magnetic beads, the lysates were incubated overnight directly. Immunoprecipitants were washed three times with the IP wash buffer (50 mM Tris–HCl, pH 7.5, 300 mM NaCl, 0.2% Triton X-100 and 10% glycerol). Proteins were eluted from the beads by boiling in SDS–PAGE loading buffer and analyzed by immunoblotting.

Immunoblotting

Cells were lysed with RIPA lysis buffer containing protease inhibitor cocktail and phosphatase inhibitor. The lysates were centrifuged at 13 000 rpm for 10 min, and the supernatants were collected to measure the protein concentration by BCA assay. After boiling with SDS loading buffer at 95°C for 10 min, the protein samples were separated by 10% SDS–PAGE and transferred to polyvinylidene fluoride (PVDF) membranes, and the membranes were blocked with Tris-buffered saline with Tween-20 (TBST) containing 5% (w/v) bovine serum albumin (BSA) prior to incubation with primary antibodies at room temperature for 2 h or 4°C overnight and secondary antibodies for 1 h at room temperature. The blots were visualized using a chemiluminescent substrate, and images were observed with an iBright 1500 imager system. Densitometry analysis was performed using ImageJ software.

Immunofluorescence

Cells were seeded on coverslips in 12-well plates and transfected with the indicated plasmids using lipofectamine 3000 as indicated. After removing the supernatants, the cells were washed with phosphate-buffered saline (PBS), fixed with 4% paraformaldehyde, permeabilized with 0.2% (v/v) Triton X-100 and blocked in 3% (w/v) BSA for 1 h. Then, the cells were incubated with the indicated primary antibodies [in 3% (w/v) BSA] overnight at 4°C followed by incubation with fluorescent secondary antibodies and 4′,6-diamidino-2-phenylindole (DAPI) for 1 h at room temperature. Finally, the coverslips were fixed on slides using aqueous mounting medium, and images were acquired with a Nikon A1RMP or Zeiss LSM710 confocal microscope. Colocalization analysis was performed using Imaris software.

In vitro cGAMP production

In vitro cGAMP production assay was performed as previously described, with minor modifications (22). Briefly, purified full-length h-cGAS (1 μM) was incubated with or without USP15 in reaction buffer (2 mM ATP, 2 mM GTP, 0.1 mg/ml herring testis (HT)-DNA, 25 mM Tris–HCl, pH 7.5, 150 mM NaCl, 5 mM $MgCl_2$, 1 μM $ZnCl_2$, 2 mM dithiothreitol (DTT) and 0.01% Tween-20] for 3 h at 28°C. The samples were then heated at 95°C for 10 min and centrifuged at 16 000 *g* for 10 min. The supernatant was analyzed by ion exchange chromatography with a HiTrap Q HP column (GE Healthcare).

Ubiquitination assay

Cells were seeded in 6-well plates, transfected with the indicated plasmids and treated with MG132 (20 μM) and CQ (20 μM) 5 h before collection. At 24 h post-transfection, cells were harvested into centrifuge tubes and lysed with buffer A (50 mM Tris–HCl pH 7.5, 150 mM NaCl, 1 mM EDTA, 10 mg/ml SDS, 0.5% NP-40 and 10% glycerol) supplemented with protease inhibitor cocktail on ice for 10 min, then a 4-fold volume of buffer B (50 mM Tris–HCl pH 7.5, 150 mM NaCl, 1 mM EDTA, 0.5% NP-40 and 10% glycerol) supplemented with protease inhibitor cocktail was added and the lysates were sonicated for 5 min in ice water until clear. The lysates were then centrifuged at 13 000 rpm for 10 min at 4°C. As in the IP assay, 60 μl of supernatant was kept as whole-cell lysate and the rest was incubated with Flag-M2 beads at 4°C overnight. Immunoprecipitants were washed three times with buffer C (50 mM Tris–HCl pH 7.5, 500 mM NaCl, 1 mM EDTA, 0.5% NP-40 and 10% glycerol), resuspended in SDS loading buffer and denatured by heating for 10 min. The immunoprecipitants were analyzed by immunoblot with the indicated antibodies (4–15% gels were used for the SDS–PAGE).

cGAMP quantification

Cells were plated in 10 cm dishes and treated or not with HT-DNA (2 μg/ml) for the indicated times before collection. Collected cells were washed with ice-cold PBS, lysed with methanol and quickly scraped into a 1.5 ml centrifuge tube, followed by five freeze–thaw cycles in liquid nitrogen. The insoluble pellet was removed by centrifugation in a cooled centrifuge (4°C), and the supernatant was transferred to a new tube and evaporated to dryness. Dried extracts were reconstituted in 80 μl of water, vortexed and centrifuged at 13 000 rpm for 10 min at 4°C, and the supernatant was centrifuged again before being loaded into the liquid chromatography–tandem mass spectrometry (LC-MS/MS) instrument for quantification. The LC-MS/MS system consisted of an ACQUITY UPLC I-Class (Waters, USA) and a QTRAP 4500 triple quadrupole mass spectrometer (AB SCIEX). An electrospray ionization source and positive ionization mode were applied. Commercial cGAMP was used as a standard sample, and the retention time was 2.56 min. The optimized ion transitions (*m/z* 675.2–524.1, 675.2–506.1) were used for quantification.

Quantitative reverse transcription–PCR (RT–qPCR)

Cells were seeded in 6-well plates and treated as indicated. Total RNA was extracted with TRIzol, and the diluted RNA was reverse transcribed using an iScript cDNA synthesis kit and analyzed via qPCR using iTaq Universal SYBR Green Supermix (on a Bio-Rad T100 thermal cycler). All reagents were used according to the manufacturer's instructions. The primers are listed in Supplementary Table S2. Glyceraldehyde phosphate dehydrogenase (GAPDH; for humans) and *β-actin* (for mice) were used as internal controls.

Live-cell imaging

USP15 and cGAS stably overexpressing cells were grown on a chambered cover glass to the correct density. After labelling, cells were transfected with fluorescence-labelled DNA using lipofectamine 3000. After 30 min, live-cell images were captured every 10 s with a ×100 oil objective, Nikon A1 camera. The images were analyzed with Imaris.

Split sfGFP complementation assay

The split superfolder green fluorescent protein (sfGFP) complementation assay was performed as previously described with minor adjustment (22). Briefly, the G10-Flag-cGAS in-frame coding sequence consists of the β-strand 10 of sfGFP MDLPDDHYLSTQTILSKDLN, a linker sequence GTDVGSGGGS, the Flag peptide DYKDDDDK, a short linker TR and human cGAS. The cGAS-HA-G11 in-frame coding sequence consists of human cGAS, a short linker VD, the hemagglutinin (HA) peptide YPYDVPDYA, a linker sequence GGGSGSGGGSGGGSTS and the β-strand 11 of sfGFP EKRDHMVLLEYVTAAGITDAS. The GFP1–9 construct was tagged with the N-terminal myc tag MEQKLISEEDL and a GSGS linker. Each of the three coding sequences were cloned into the pTY lentiviral vector with puromycin resistance. After simultaneous lentiviral transduction of all three constructs, stable HEK293T cells were selected in 2 μg/ml puromycin. Protein stable expression was verified by western blotting using Flag, Myc or HA antibodies. GFP formation in the resulting cell lines was observed by confocal fluorescence microscopy.

Recombinant proteins of the three constructs were expressed and purified from *E. coli*. To test fluorescence complementation *in vitro*, the three components and Cy5-labeled ISD or 100 bp DNA were mixed at the concentration of 5 μM each in a buffer of 20 mM Tris–HCl, pH 7.5, 5 mM $MgCl_2$, 100 mM NaCl and 1 mg/ml BSA. GFP intensity were measured in a clear-bottom 96-well plate with a Varioskan Flash microplate reader (Thermo Scientific), performing scans at 60 s intervals for 120 min. At the end of incubation, the level of phase separation was observed under confocal fluorescence microscopy. To test the effect of USP15 on cGAS activation, the mixture was either supplemented or not with 2 μM recombinant USP15.

In vitro phase separation

In general, 2 μM of recombinant cGAS protein (2% fluorescence labelled) or cGAS–enhanced GFP (EGFP) was mixed with 2 μM DNA of a defined length (2% Cy5 labeled) in 96-well plates (Corning) in a buffer containing 20 mM Tris–HCl, pH 7.5, 5 mM $MgCl_2$, 150 mM NaCl and 1 mg/ml BSA. Mixtures were incubated and images were captured at the indicated times. Phase separation in the presence or absence of USP15 was performed by mixing fluorescence-labelled recombinant USP15 (275–981) with Cy5-labeled DNA in buffer containing 20 mM Tris–HCl, pH 7.5, 150 mM NaCl and 1 mg/ml BSA. At the end of incubation, the formation of liquid droplets was observed under light microscopy.

In vitro FRAP assays

In vitro fluorescence recovery after photobleaching (FRAP) assays were performed as previously described with minor adjustments (23). FRAP experiments were performed with a Nikon A1RMP confocal microscope at room temperature. USP15 spots of ∼1 μm diameter were photobleached with 10% laser power for 0.5 s using 488 nm or 561 nm lasers. Time-lapse images were acquired over a 10 min time course after bleaching at 6 s intervals. The fluorescence intensities of regions of interest (ROIs) were corrected by unbleached control regions and then normalized to the prebleached intensities of the ROIs. The corrected and normalized data were fit to the single exponential model by GraphPad Prism 7.

Statistical analyses

GraphPad Prism 7 software was applied to perform statistical analyses. All experiments were performed with at least triplicate samples as independent biological replicates. Two-tailed Student's *t*-test was used to compare data points. Significance levels are shown with asterisks, as follows: $*P < 0.05$; $**P < 0.01$; and $***P < 0.001$. Data with error bars are presented as the mean values with the standard error of the mean (SEM).

RESULTS

USP15 interacts with cGAS

To dissect the molecular mechanism by which cGAS activation is regulated, we overexpressed Flag epitope-tagged cGAS in HEK293T cells and performed IP combined with LC-MS/MS to identify proteins that interact with cGAS. We found several interesting proteins, including USP15 (Supplementary Figure S1A), which has been recently reported to play critical roles in regulating immune and inflammatory responses (19–20,24–26). To confirm that USP15 interacts with cGAS, we overexpressed Flag-epitope tagged USP15 and Myc epitope-tagged cGAS and performed co-IP experiments. We found that USP15 pulled down cGAS (Figure 1A). Consistently, Flag epitope-tagged cGAS also pulled down Myc epitope-tagged USP15 (Figure 1B), indicating an association between cGAS and USP15. To confirm a direct interaction between cGAS and USP15, we performed GST pull-down experiments using recombinant GST-tagged cGAS and USP15 (Supplementary Figure S1B). GST-tagged cGAS, but not the negative control GST protein, pulled down recombinant USP15 (Figure 1C). Consistently, GST-tagged USP15 (521–981) pulled down recombinant cGAS (Figure 1D), indicating a direct interaction between USP15 and cGAS.

To identify the domains that are essential in the cGAS–USP15 interaction. We constructed several truncation mutants and employed them in the co-IP experiments (Figure 1E). USP15 consists of several domains: a DUSP domain, two UBL domains, two DUB domains and a linker region. We found that the two DUB domains and the linker region were necessary for USP15 interaction with cGAS (Figure 1E, F). We found that these domains and linker region are highly conserved in vertebrates (Supplementary Figure S1B). CGAS consists of two important regions: the N-terminal domain (NTD) is important for DNA binding, and the C-terminal domain (CTD) is essential for its enzymatic activity (Figure 1G). In the co-IP experiments, both the NTD and CTD showed the ability to bind USP15, with the NTD showing a stronger association with USP15 (Figure 1H). To assess how cGAS and USP15 interact with each other at the subcellular level, we overexpressed HA-tagged cGAS and Myc-tagged USP in cGAS-KO HeLa cells and detected their cellular distribution. USP15 and cGAS clearly co-localized with each other, indicating a strong association between USP15 and cGAS in cells (Figure 1I). Moreover, to determine the physiological association between USP15 and cGAS, we performed an endogenous IP experiment in Raw264.7 cells. USP15 and cGAS pulled each other down when both were in a resting state and in the presence of HT-DNA, a long dsDNA widely used to activate cGAS (27) (Figure 1J; Supplementary Figure S1C). Taken together, these results suggest that USP15 physically interacts with cGAS.

USP15 positively regulated cGAS activation in a feedback loop

Considering that USP15 plays important roles in many innate immune signal transduction pathways (19–20,24–26), we suspected that USP15 also functions in cGAS/STING-mediated innate immune responses. To test this hypothesis, we transfected THP-1 cells with HT-DNA to activate cGAS (27). HT-DNA strongly induced IFNβ expression, indicating cGAS/STING signaling activation (Figure 2A). In addition, the USP15 mRNA level was also increased in cells transfected with HT-DNA (Figure 2B), indicating that USP15 expression was induced by cGAS/STING signaling. To verify this outcome, we infected L929 cells with vaccinia virus (VACV), which has been reported to activate cGAS/STING signaling (28). Phosphorylation of STING was increased 12 and 24 h post-VACV infection, indicating cGAS/STING signaling activation (Figure 2C). We also found that the protein expression levels of cGAS and USP15 were increased, confirming that USP15 expression was induced by cGAS/STING signaling activation (Figure 2C), which was consistent with the result in Raw264.7 cells (Supplementary Figure S1C). Taken together, these results indicated that cGAS/STING signaling activation induced USP15 expression.

To better understand whether USP15 functions in cGAS-mediated innate immune responses, we established an L929 cell line stably overexpressing USP15 (Figure 2D). After transfection with HT-DNA, the USP15-overexpressing cells showed higher *Ifnβ* and *Cxcl10* expression, indicating a positive role for USP15 in cGAS activation (Figure 2E, F). To confirm this result, we depleted the expression of USP15 in Raw264.7 cells using the CRISPR/Cas9 genome editing system. The USP15 protein expression level was successfully reduced (Supplementary Figure S2C). Moreover, we examined the endogenous cGAMP production in wild-type and USP15-depleted cells after DNA stimulation. The result showed that depletion of USP15 completely abolished endogenous cGAMP production stimulated by HT-DNA, indicating the physiological role of USP15 in cGAS activation (Figure 2G). Consistently, compared with those in control cells under the same conditions, low USP15 protein expression levels dampened HT-DNA-induced *Ifnb1*, *Tnfa* and *Il6* expression, indicating a positive role for endogenous USP15 in regulating cGAS activation (Figure 2H–J). Furthermore, we sought to determine whether USP15 directly affects cGAS enzyme activity *in vitro*. As shown by the ion exchange chromatography data, cGAS consumed ATP and GTP to produce cGAMP in the presence of HT-DNA (Figure 2K). When USP15 was added, the production of cGAMP increased 3 and 6 h post-reaction, indicating that USP15 directly promoted cGAS enzyme activity. Additionally, we confirmed the role played by USP15 in other innate immune pathways. Sendai virus (SeV) dramatically induces the production of type I IFNs and inflammatory cytokines through the RIG-I–MAVS (mitochondrial antiviral signaling protein) signaling pathway. In this study, knocking out USP15 expression enhanced *Ifnb1* and *Il6* expression, indicating a negative role played by USP15 in RNA sensing (Supplementary Figure S2D, E). Moreover, we used lipopolysaccharide (LPS) and R848 to activate TLR4 and TLR7/8, respectively. USP15 KO substantially inhibited *Ifnb1* and *Tnfa* expression (Supplementary Figure S2F–I), suggesting that USP15 played a positive role in TLR4 and TLR7/8 signaling transduction. We also stimulated USP15-depleted cells with cGAMP directly to activate STING signal. The results showed that cGAMP induced

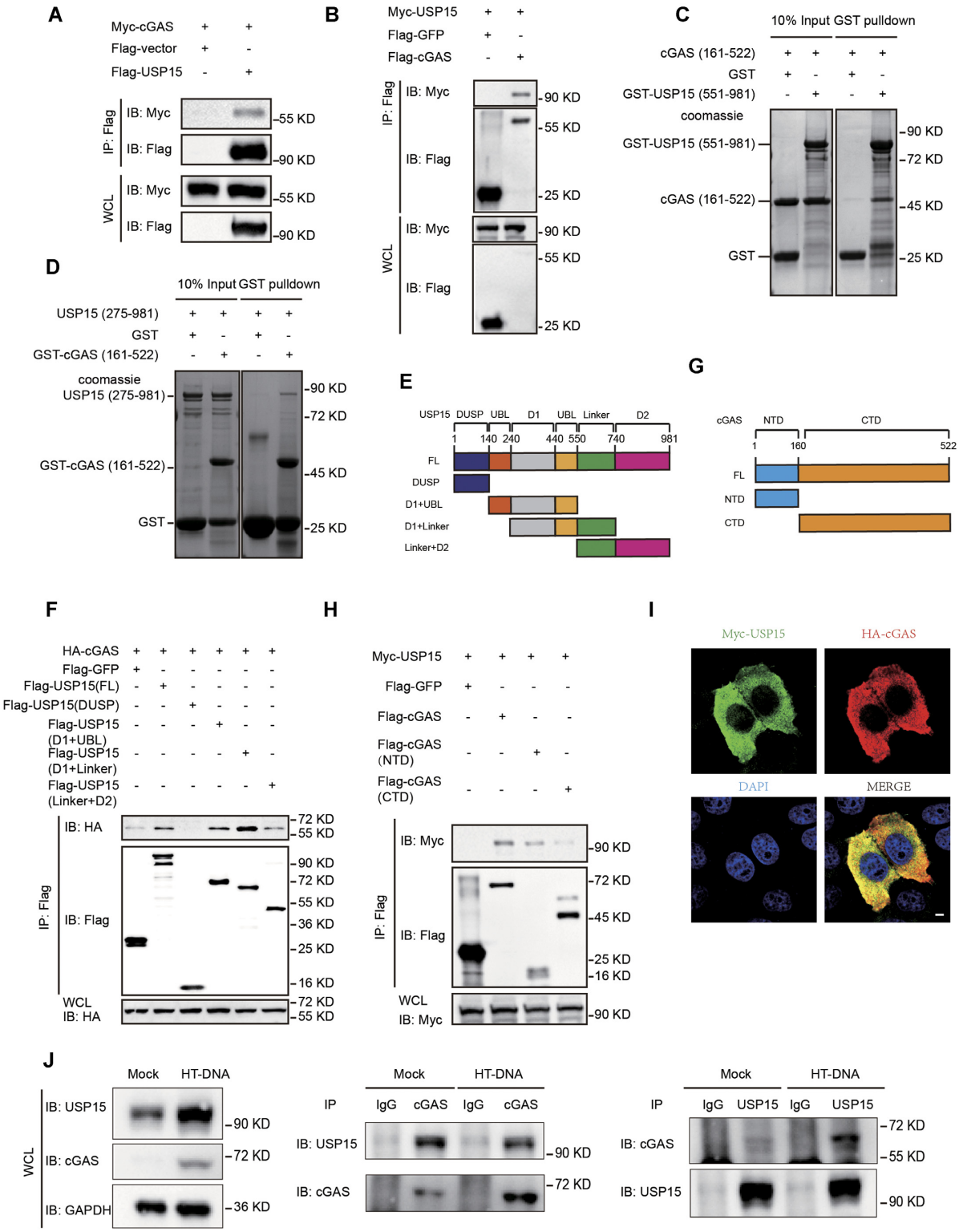

Figure 1. USP15 interacts with cGAS. (**A** and **B**) Immunoprecipitation (with an anti-Flag antibody) and immunoblot analysis of HEK293T cells transfected with the indicated plasmids for 24 h. WCL, whole-cell lysate; IP, immunoprecipitation. (**C** and **D**) GST precipitation assay of GST or GST-tagged USP15 (551–981) (C) or GST–cGAS (161–522) (D) incubated for 4 h with cGAS (161–522) (C) or USP15 (275–981) (D), as assessed with Coomassie blue staining. (**E**) Schematic diagrams showing USP15 and truncation mutants. (**F**) Immunoprecipitation (with an anti-Flag antibody) and immunoblot analysis of HEK293T cells transfected with plasmids encoding HA-cGAS and Flag-USP15 truncations or GFP for 24 h. (**G**) Schematic diagrams showing cGAS and truncation mutants. (**H**) Immunoprecipitation (with an anti-Flag antibody) and immunoblot analysis of HEK293T cells transfected with plasmids encoding Myc-USP15 and Flag-cGAS truncation mutants or GFP for 24 h. (**I**) Immunofluorescence analysis of HA-cGAS (red) and Myc-USP15 (green) in cGAS knockout HeLa cells. Scale bars: 5 μm. (**J**) Immunoprecipitation (with IgG, an anti-cGAS antibody or an anti-USP15 antibody) and immunoblot analysis of Raw264.7 cells transfected with or without HT-DNA for 12 h. Data are representative of at least two independent experiments.

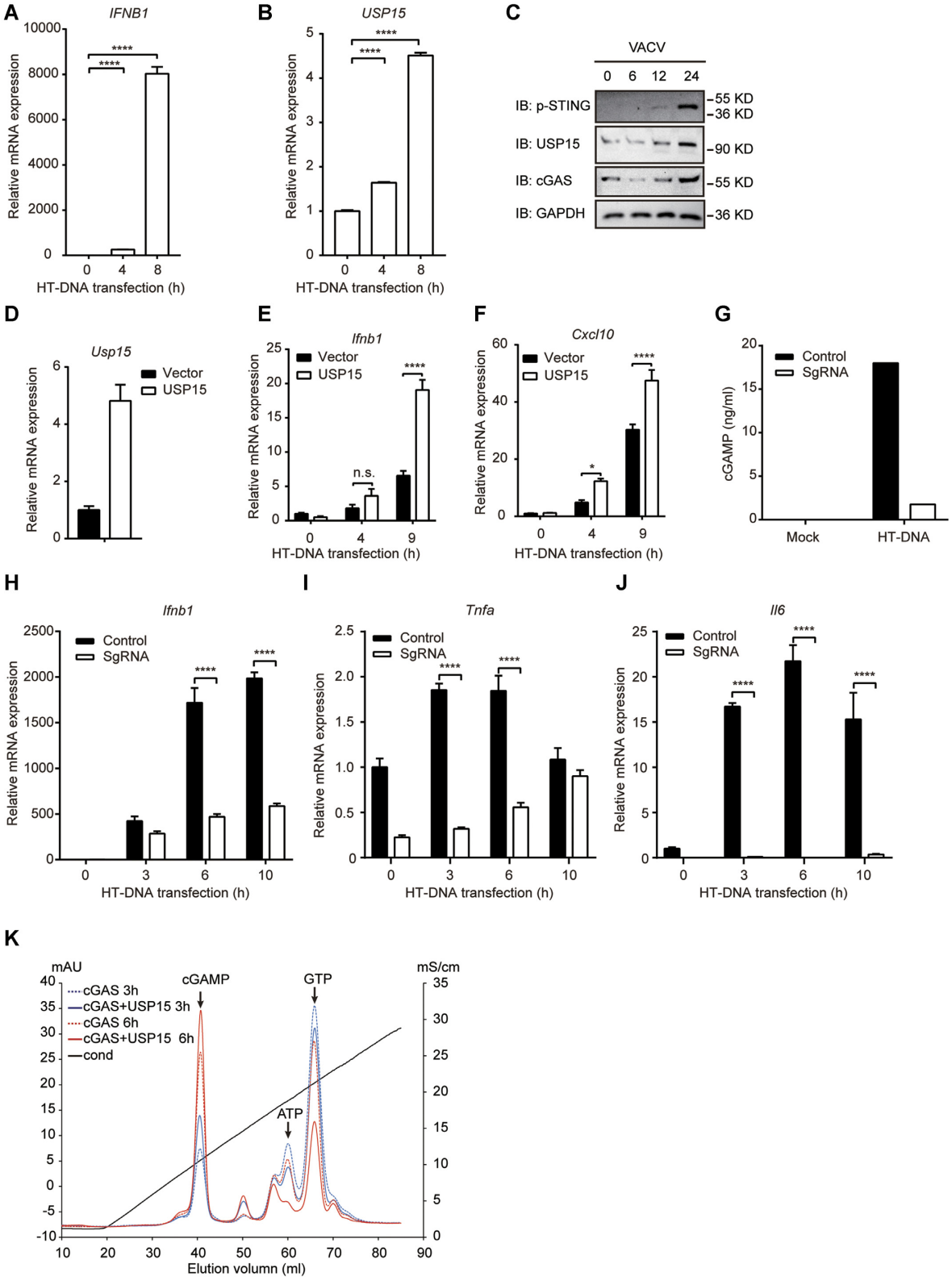

Figure 2. USP15 promotes cGAS-mediated innate immune responses in a positive feedback manner. (**A** and **B**) THP-1 cells were transfected with HT-DNA (2 μg/ml) for the indicated times before RT–qPCR analysis of *IFNB1* and *USP15* expression. (**C**) MEFs were infected with VACV for the indicated time before western blot analysis of USP15, p-STING and cGAS. (**D**–**F**) Control or stably USP15 overexpressing L929 cells were transfected with HT-DNA (2 μg/ml) for the indicated times before RT–qPCR analysis of *Usp15* (D), *Ifnb1* (E) or *Cxcl10* (F) expression. (**G**) Control and Usp15-KO Raw264.7 cells were transfected with HT-DNA (2 μg/ml) for 4 h before measurement of endogenous cGAMP. (**H**–**J**) Control and Usp15-KO Raw264.7 cells were treated with HT-DNA (2 μg/ml) for the indicated time before RT–qPCR analysis of *Ifnb1* (H), *TNFa* (I) or *Il6* (J). (**K**) An *in vitro* cGAMP production assay was performed for the indicated times with or without USP15. The data are representative of at least two independent experiments; mean ± SEM from triplicates of technical replicates, unpaired *t*-test; n.s., not significant; **P* <0.05; *****P* <0.0001.

expression of *Ifnb1* and *Il6* in control cells, confirming the activation of STING (Supplementary Figure S2J, K). Interestingly, depletion of USP15 abolished the expression of both *Ifnb1* and *Il6*, indicating that USP15 was also essential for STING signal transduction (Supplementary Figure S2J, K). Consistent results were obtained when we detected the level of TBK1 and IRF3 phosphorylation induced by cGAMP, LPS or SeV in USP15-depleted cells, indicating that USP15 played heterogenous roles in different pathways (Supplementary Figure S2L–N). Collectively, these results indicated that USP15 positively regulated cGAS activation through a feedback loop.

USP15-mediated deubiquitylation promotes cGAS activation

To determine the molecular mechanism by which cGAS activity is regulated by USP15, we preliminarily focused on cGAS ubiquitination. We performed a ubiquitination assay and found that overexpressed cGAS was ubiquitinated in HEK293T cells (Figure 3A). When both USP15 and cGAS were overexpressed, the level of cGAS ubiquitination was dramatically reduced (Figure 3A), indicating that USP15 may deubiquitylate cGAS. To confirm USP15 deubiquitylation on cGAS, we constructed a USP15 C298A mutant (an enzymatic dead mutant with a cysteine to alanine amino acid substitution at residue 298). In the ubiquitination assay, the ubiquitination level of cGAS was recovered when the USP15 C298A mutant and cGAS were both overexpressed, which confirmed that USP15 enzyme activity was essential in regulating cGAS deubiquitylation (Figure 3A). Ubiquitin can be linked to proteins through K6–, K11–, K27-, K29–, K33–, K48– and K63–ubiquitin linkages (29). To determine which of the lysine modifications that link ubiquitin to cGAS are regulated by USP15, we subjected cGAS with various ubiquitinated constructs to ubiquitination assay and found that cGAS undergoes polyubiquitination through all the aforementioned ubiquitin–lysine linkages (Figure 3B). Overexpression of USP15 reduced cGAS ubiquitination. Moreover, the USP15 C298A mutant failed to deubiquitylate cGAS (Figure 3B). In our study (unpublished data), we found that cGAS was ubiquitinated at K231, K258 and K392. To determine whether USP15-mediated deubiquitylation affected these lysine sites, we constructed K231R, K258R and K392R cGAS mutants and studied them in ubiquitination assays. As shown in Supplementary Figure S3A, USP15 showed no regulatory effect on these cGAS mutants, indicating that USP15 may function at all these cGAS lysine sites. Moreover, based on our previous work showing that the E3 ligase MARCH8 promoted K63-linked polyubiquitination of cGAS (30), we found that USP15 deubiquitylated MARCH8-mediated cGAS polyubiquitination (Supplementary Figure S3B). To confirm the ubiquitination sites of USP15-mediated deubiquitylation, we constructed a K231R/K258R/K392R mutant and employed it in the ubiquitination assay. The result showed that the K231R/K258R/K392R mutant failed to be ubiquitinated by MARCH8 and deubiquitinated by USP15 (Figure 3C). Moreover, to determine the physiological regulation of cGAS ubiquitination, we examined the ubiquitination level of cGAS in wild-type and USP15-depleted cells. The result showed that depletion of USP15 markedly enhanced endogenous ubiquitination of cGAS (Figure 3D). Both endogenous K48- and K63-linked polyubiquitination of cGAS were enhanced in USP15-depleted cells, consistent with the result in overexpression experiments (Supplementary Figure S3C). To understand the role of deubiquitylation in cGAS activation, we overexpressed cGAS in HEK293T cells and measured the concentration of cGAMP, the product of cGAS activation. As shown in Figure 3E, co-overexpression of USP15 and cGAS led to increased cGAMP production, whereas the USP15 C298A mutant rescued cGAMP production, indicating that USP15 deubiquitylation activity was important in enhancing cGAS activation (Figure 3E). Moreover, we asked whether USP15 kept cGAS from being degraded by performing a protein stability assay. We overexpressed cGAS in HEK293T cells and treated cells with cycloheximide (CHX) to inhibit protein synthesis. The result showed that USP15 did not influence the degradation of cGAS (Supplementary Figure S3D). We also asked whether USP15 affected other key players in the pathway that affect cGAS or even cGAMP directly. We focused on ENPP1, which is a cGAMP degradation enzyme (31). We used small interfering RNA (siRNA) to knock down USP15 in THP-1 cells and detected the protein level of ENPP1 (Supplementary Figure S3E). The result showed that the protein level of ENPP1 was not affected after USP15 knockdown, indicating that USP15 did not affect the level of cGAMP (Supplementary Figure S3E). Taken together, these results suggest that USP15-mediated deubiquitylation of cGAS is essential for cGAS activation.

USP15 promotes DNA-induced oligomerization and phase separation of cGAS

Because DNA binds to cGAS and induces its dimerization, oligomerization and liquid condensation, which facilitate cGAMP production (1,32–35), we examined whether USP15 affects the DNA binding ability of cGAS. Since ISD, with 45 bp, is a commonly used cGAS stimulator, we firstly mixed EGFP–cGAS with Cy5-labeled ISD and observed the formation of liquid droplets (Supplementary Figure S3F). Then we overexpressed cGAS in HEK293T cells and performed an ISD pull-down assay. The cGAS band in the ISD IP assay indicated an interaction between cGAS and ISD (Figure 4A). When USP15 was overexpressed with cGAS, cGAS abundance increased, indicating that USP15 promoted the cGAS–DNA binding (Figure 4A). Interestingly, when we subjected the USP15 C298A mutant to this assay, the cGAS band was almost the same as that of the wild-type control, indicating that the regulatory effect of USP15 on cGAS–DNA binding was not dependent on deubiquitylation activity (Figure 4A). Furthermore, cGAS dimerization induced by DNA was also increased when USP15 and cGAS were both overexpressed (Supplementary Figure S4A).

To better understand the detailed mechanism by which USP15 promotes the DNA–cGAS interaction and subsequent cGAS dimerization, we established a split GFP complementation reporter system (22). sfGFP was split into three parts: a GFP 1–9 β-sheet assembly (GFP1–9), a 10 β-

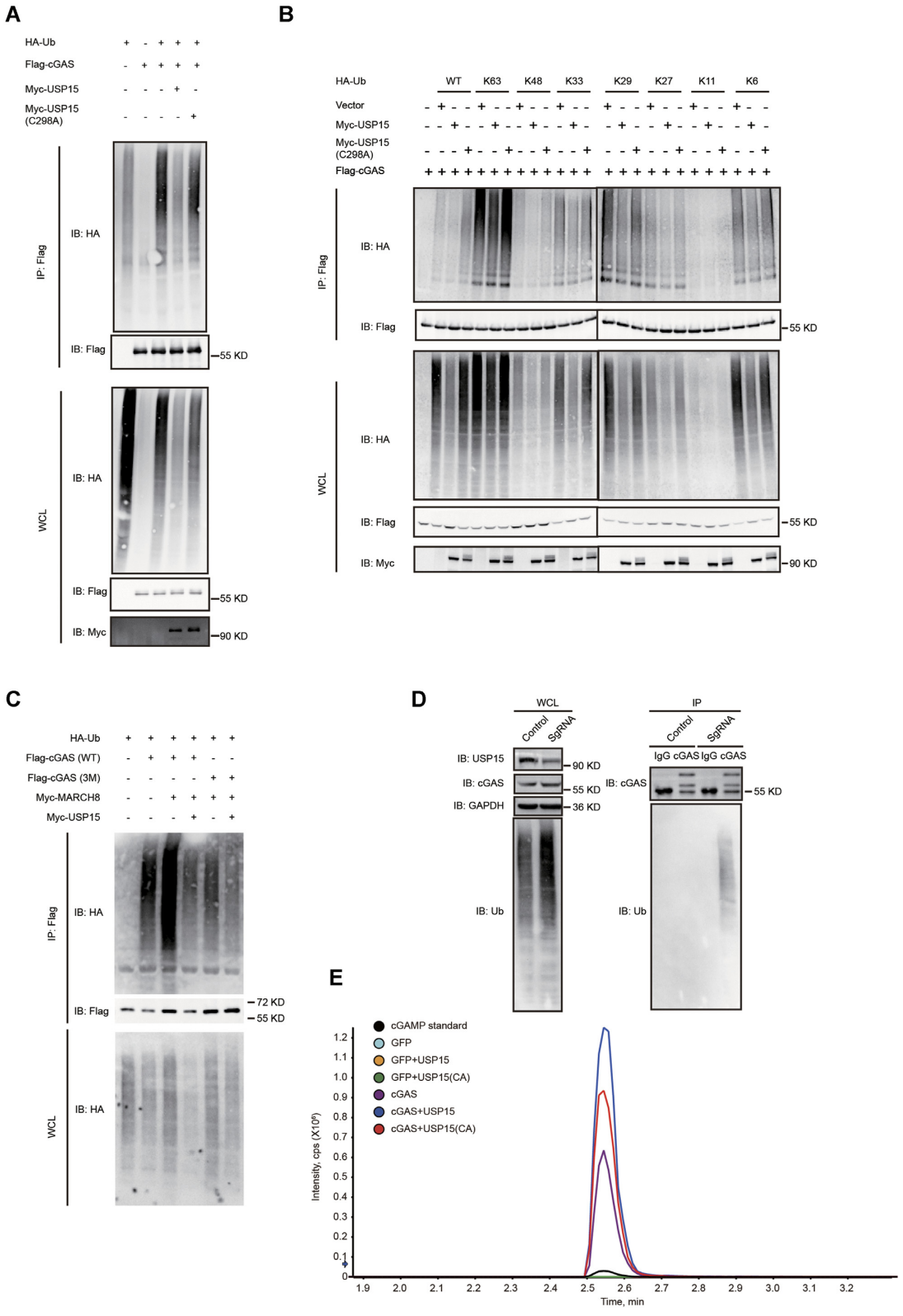

Figure 3. USP15-mediated deubiquitylation is important for cGAS activation. (**A**) HEK293T cells were transfected with Flag-cGAS, HA-Ub and Myc-USP15 or Myc-USP15 (C298A) for 24 h before ubiquitination assays were performed. WCL, whole-cell lysate; IP, immunoprecipitation. (**B**) HEK293T cells were transfected with Flag-cGAS, HA-Ub [wild type (WT), K6, K11, K27, K29, K33, K48 or K63] and Myc-USP15 or Myc-USP15 (C298A) for 24 h before ubiquitination assays were performed. (**C**) HEK293T cells were transfected with Flag-cGAS (WT or mutant), HA-Ub, Myc-MARCH8 and Myc-USP15 for 24 h before ubiquitination assays were performed. 3M, a mutant with K231R, K258R and K392R substitution of cGAS. (**D**) An endogenous ubiquitination assay was performed in control and Usp15-KO Raw264.7 cells. (**E**) HEK293T cells were transfected with the indicated plasmids, and the amount of cGAMP in the lysates was quantified by LC-MS/MS. The data are representative of at least two independent experiments.

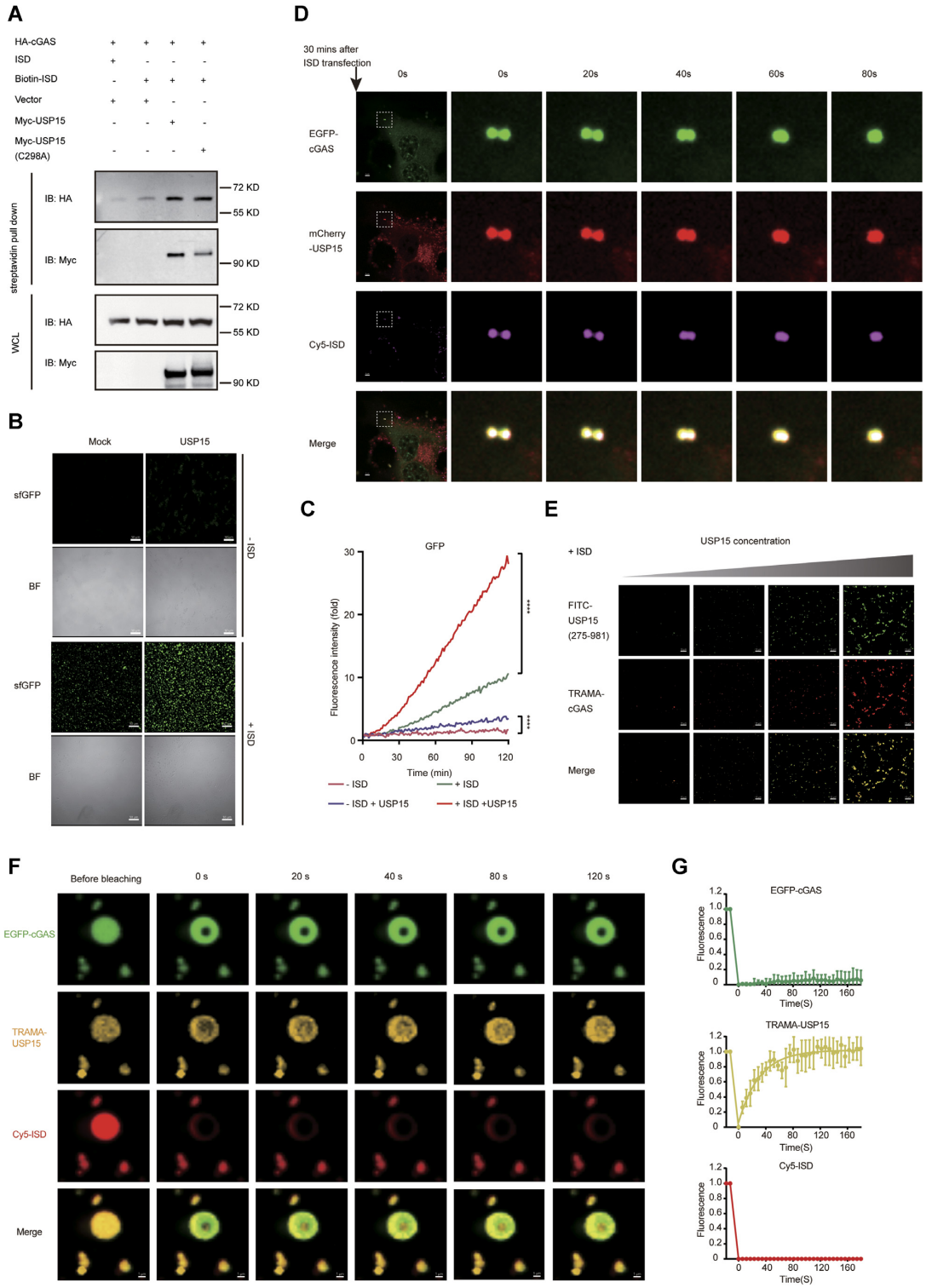

Figure 4. USP15 promotes DNA-induced cGAS oligomerization and phase separation. (**A**) HEK293T cells were transfected with the indicated plasmids. Biotin-conjugated ISD was transfected into cells 6 h before harvesting. Lysates were co-precipitated with streptavidin beads and then assessed by immunoblot analysis as shown. WCL, whole-cell lysate; IP, immunoprecipitation. (**B**) The split sfGFP complementation system with the addition of USP15 with (bottom) or without (top) ISD. Scale bar: 50 μm. (**C**) GFP intensity of split sfGFP as shown in (B). (**D**) HeLa cells stably expressing EGFP–cGAS and mCherry–USP15 were transfected with Cy5–ISD. Images were taken every 10 s at 30 min after ISD transfection. Scale bar: 3 μm. (**E**) Image showing fluorescein isothiocyanate (FITC)-labeled USP15 (275–981) (0.1, 0.5, 1, 2 μM) and TAMRA-labeled cGAS (1 μM) in the presence of ISD (2 μM). (**F** and **G**) FRAP of EGFP–cGAS, TAMRA-labeled USP15 and Cy5-labeled ISD in the cGAS/USP15/DNA condensates. Bleaching was performed 60 min after mixing EGFP–cGAS (5 μM), TAMRA–USP15 (5 μM) and Cy5–ISD (5 μM). Time 0 indicates the end of photobleaching and the start of recovery. The means ± standard deviation (SD) are shown. $n = 4$ liquid droplets. The images shown in (F) are representative images of the FRAP assay of the liquid droplets. The data are representative of at least two independent experiments

sheet assembly fused to the N-terminus of cGAS and an 11 β-sheet assembly fused in the C-terminus of cGAS (Supplementary Figure S4B, C). In the absence of DNA, the cGAS monomers separate from each other but, with the addition of DNA, cGAS bound to DNA and formed dimerized structures (34,36). In our sfGFP complementation reporter system, no GFP signal was detected when we mixed purified G_{10}–cGAS and cGAS–G_{11} with $sfGFP_{1–9}$ without DNA, indicating that the two monomers were separated (Figure 4B, C). When we added ISD to the system, the GFP fluorescence intensity increased ∼10-fold, indicating that DNA induced the binding of the G_{10}–cGAS monomer and cGAS–G_{11} monomer (Figure 4B, C). In particular, when the concentration of NaCl salt in the system was 100 mM, sfGFP presented with a punctate pattern, indicating that the tripartite split GFP reporter system was a good indicator of cGAS dimerization and oligomerization (Supplementary Figure S4D, E). With the addition of USP15, the sfGFP signal was greatly increased in the presence of DNA, indicating that USP15 promoted DNA-induced cGAS oligomerization and phase separation (Figure 4B, C). Interestingly, we found that the addition of USP15 also increased the GFP signal even in the absence of DNA (Figure 4B, C), implying that USP15 played a role in promoting cGAS dimerization and phase separation *in vitro*. To determine whether these outcomes can be induced in the physiological environment, we stably overexpressed EGFP–cGAS and mCherry–USP15 in HeLa cells. After transfection with Cy5-labeled ISD, liquid droplets containing cGAS and DNA appeared ∼30 min post-transfection (Figure 4D). The liquid droplets fused into a larger droplet over time, indicating the dynamic molecular exchange caused by cGAS phase separation induced by DNA in these cells (Figure 4D). We found that USP15 was involved in the entire puncta fusion process, implying that USP15 played a role in cGAS phase separation in these cells. To confirm this hypothesis, we induced liquid condensation of cGAS and DNA *in vitro* (Figure 4E). As shown in Figure 4E, USP15 fused with cGAS–DNA puncta *in vitro*. Moreover, an increase in USP15 concentration dramatically promoted liquid condensation of cGAS and DNA (Figure 4E; Supplementary Figure S4F). To determine whether USP15 in the droplets also underwent phase separation, we performed a FRAP assay. The fluorescence of TAMRA-labelled USP15 quickly recovered within 80 s post-photobleaching, whereas fluorescence of cGAS and ISD hardly recovered (Figure 4F, G). The result indicated that USP15, but not cGAS or DNA, in the cGAS–DNA droplets was dynamic and changing with the environment, typical of molecules undergoing phase separation (Figure 4F, G). Taken together, these results indicated that USP15 promoted DNA-induced cGAS oligomerization and liquid condensation.

The USP15 IDR promotes cGAS liquid condensation and activation

To further study the molecular mechanism of USP15-driven cGAS oligomerization and liquid condensation, we first analyzed the amino acid composition of USP15. We found that USP15 contains a conserved IDR from amino acids 620 to 700 (Supplementary Figure S5A). The region consists of many aspartic acid and glutamic acid residues and exhibits a negative charge (Figure 5A). Because the cGAS N-terminus, which consists of many positively charged amino acids, is critical for liquid condensation through multivalent interactions in the presence of DNA (23), we speculated that the valency of the interaction between the negatively charged IDR of USP15 and the positively charged N-terminal domain of cGAS contributed to the liquid condensation of cGAS (Figure 5B). To test this hypothesis, we purified recombinant USP15 protein in which the IDR was deleted and employed it with a split GFP complementation reporter system. The results showed that the addition of USP15 enhanced the GFP signal with or without the presence of DNA but the IDR-deleted mutant failed to do so (Supplementary Figure S5B, C), indicating that the USP15 IDR is important in promoting cGAS dimerization and oligomerization.

Moreover, we asked whether this outcome is evident in HEK293T cells stably overexpressing these three parts of sfGFP–cGAS. In the absence of DNA, cGAS monomers separated from each other and exhibited autoinhibition (33,34). In addition, the split GFP reporter did not exhibit a GFP signal in the cytoplasm. Interestingly, a GFP signal appeared in cells overexpressing USP15, indicating that USP15 promotes the binding of GFP_{10}–cGAS and cGAS–GFP_{11}, even in the absence of DNA (Figure 5C). Moreover, in the presence of DNA, GFP puncta appeared in the cytoplasm, suggesting DNA-induced cGAS dimerization and phase separation. When USP15 was overexpressed, the mean GFP fluorescence intensity of the puncta substantially increased, suggesting that USP15 promotes cGAS oligomerization (Figure 5C, D). However, after deletion of the IDR, the mean GFP intensity in the puncta was reduced, indicating that the IDR in USP15 plays an important role in cGAS dimerization and phase separation (Figure 5C, D). Furthermore, when we mixed EGFP-fused cGAS and USP15 *in vitro*, we found that USP15 promoted the formation of cGAS liquid droplets. However, after the IDR was deleted, USP15 failed to drive cGAS condensation, indicating that the IDR in USP15 directly promoted liquid cGAS condensation *in vitro* (Figure 5E). Consistently, the interaction between cGAS and USP15 became weaker after the IDR of USP15 was deleted (Supplementary Figure S5D). We also conducted a GST pull-down assay and found that deletion of the IDR completely abolished the interaction between cGAS and USP15, indicating that the IDR of USP15 was important for its direct binding with cGAS (Supplementary Figure S5E). Taken together, these results suggest that the IDR in USP15 promoted cGAS oligomerization and liquid condensation.

Considering the aforementioned results, we sought to determine the relationship between USP15-driven cGAS deubiquitylation and cGAS liquid condensation. First, our obtained data showed that both the wild-type USP15 and the USP15 C298A mutant promoted cGAS DNA binding ability and dimerization (Figure 4A; Supplementary Figure S4A), indicating that DNA-induced cGAS oligomerization or phase separation was not dependent on cGAS deubiquitylation mediated by USP15. Next, we asked whether USP15-mediated cGAS liquid condensation affected the cGAS ubiquitination level. We employed the ΔIDR mu-

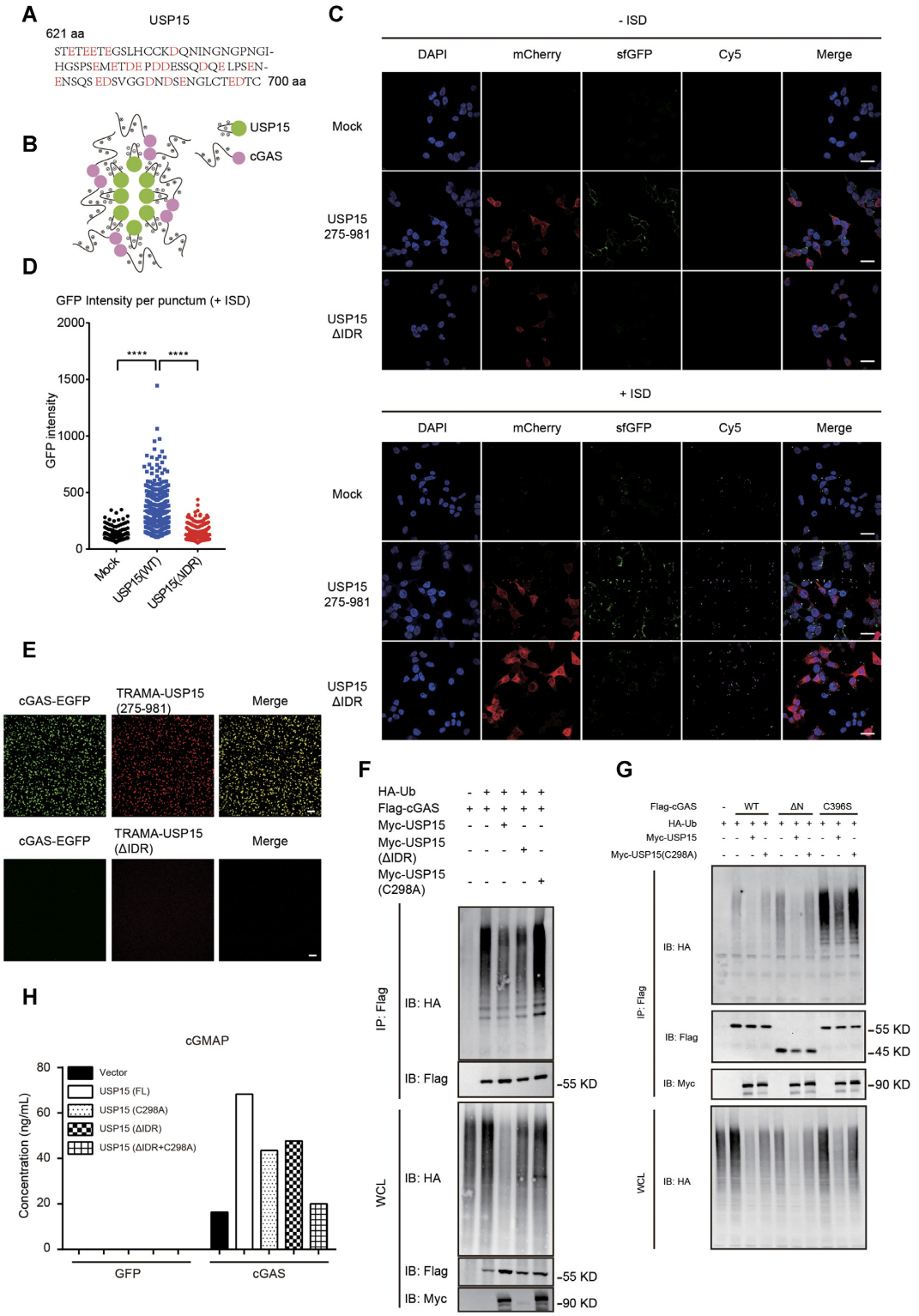

Figure 5. The IDR of USP15 promotes liquid–liquid phase separation of cGAS. (**A**) The peptide of USP15 containing amino acids 621–700. Red indicates negatively charged residues. (**B**) Schematic showing the hypothetical cGAS and USP15 valences. (**C**) Representative fluorescence microscopy images showing the complementation of split sfGFP in HEK293T cells stably expressing G10-Flag-cGAS, cGAS-HA-G11, GFP1–9 and USP15 (FL) or USP15 (ΔIDR) with (bottom) or without (top) DNA. (**D**) GFP intensity of the split sfGFP in HEK293T cells as shown in (C). (**E**) TAMRA was used to label cGAS–EGFP (2 μM), USP15 (2 μM) or USP15 (ΔIDR) (2 μM) for 30 min before microscopy imaging. Scale bar: 5 μm. (**F**) HEK293T cells were transfected with Flag-cGAS, HA-Ub and Myc-USP15 (WT, ΔIDR, C298A) for 24 h before ubiquitination assays. WCL, whole-cell lysate; IP, immunoprecipitation. (**G**) HEK293T cells were transfected with Flag-cGAS (WT, ΔN or C396S), HA-Ub and Myc-USP15 or Myc-USP15 (C298A) for 24 h before ubiquitination assays were performed. (**H**) HEK293T cells were transfected with the indicated plasmids, and the amount of cGAMP in the lysates was quantified by LC-MS/MS. The data are representative of at least two independent experiments.

tant in a ubiquitination assay and found that USP15 with the IDR deleted and wild-type USP15 had the same effect on cGAS under the same conditions, whereas the USP15 C298A mutant clearly recovered cGAS ubiquitination (Figure 5F). These data indicated that the IDR in USP15 played an important role in the cGAS oligomerization and liquid condensation but did not contribute to the cGAS deubiquitylation. Moreover, we constructed two other cGAS constructs. The one with deletion of the N-terminus failed to form liquid–liquid phase separation with DNA (37). We also constructed a mutant with a substitution of C396S, which is located in site A of the DNA-binding surface (34,36). The C396S mutant failed to bind DNA and form high ordered oligomerization (34,36). We further examined the activity of the two mutants and found that both mutants produced negligible amounts of cGAMP in cells, indicating the essential role of DNA binding and phase separation for cGAS activation (Supplementary Figure S5F). However, both mutants were deubiquitylated by USP15, suggesting that cGAS deubiquitylation mediated by USP15 is not dependent on DNA-induced cGAS oligomerization or phase separation (Figure 5G). Furthermore, we assessed the contribution of USP15-mediated deubiquitylation and phase separation to cGAS activation by measuring the production of cGAMP in cGAS-overexpressing HEK293T cells. As shown in Figure 5H, full-length USP15 dramatically enhanced cGAMP production, which was consistent with the previously obtained results. In contrast to wild-type USP15, both the C298A mutant, which failed to deubiquitylate cGAS, and the IDR deletion mutant, which failed to promote cGAS liquid condensation, partially reduced cGAMP production, indicating that both USP15-mediated deubiquitylation and liquid condensation are essential for cGAS activation (Figure 5H). Importantly, the mutant with both C298A substitution and deletion of the IDR completely abolished the enhancement of cGAMP production, indicating that USP15-mediated cGAS deubiquitylation and liquid condensation are sufficient for USP15-mediated cGAS activation (Figure 5H). To further conform this result, we reconstituted the expression of USP15 wild type, catalytically inactive or IDR-deleted mutants of USP15 into USP15-depleted cells and tested the responses to DNA stimulation (Supplementary Figure S5G, H). We found that deletion of USP15 abolished the expression of type I IFNs (Supplementary Figure S5G, H). Reconstitution of USP15 wild type, but not catalytically inactive or IDR-deleted mutants of USP15, rescued the expression of *Cxcl10* and *Ifnb1* (Supplementary Figure S5G, H). Consistently, an in *vitro* cGAMP production assay showed the importance of the USP15 IDR in cGAS activity (Supplementary Figure S5I, J). Taken together, these results indicate that USP15-mediated cGAS deubiquitylation and liquid condensation are two parallel mechanisms that are both essential and sufficient for cGAS activation.

DISCUSSION

cGAS is a non-redundant cytosolic DNA sensor that produces type I IFNs and proinflammatory cytokines through the STING/TBK1/IRF3 axis. cGAS plays essential roles in antiviral processes, antitumor immune responses and autoimmune diseases. Inactivation of cGAS typically always leads to silenced innate immune responses, whereas aberrant activation of cGAS may cause autoimmune or chronic inflammatory diseases. Therefore, cGAS activity must be properly regulated. However, the mechanism by which cGAS activation is regulated remains to be fully understood.

USP15-mediated deubiquitylation has been previously reported to play important roles in different molecular processes, including antitumor immunity, bacterial infection and transforming growth factor-β (TGF-β) signal transduction (38–41). In antiviral signal transduction, USP15 can enhance RIG-I signaling by deubiquitylating TRIM25, a process that is also required for neuroinflammation pathogenesis (17,18). USP15 in tandem with TRIM25 positively regulates type I IFN responses and promotes pathogenesis during neuroinflammation in a MAVS-independent manner. However, despite a high probability that USP15 plays a role in the DNA-induced cGAS/STING signaling pathway, the evidence remains elusive.

In this study, by overexpressing and knocking out USP15 expression, we confirmed that USP15 plays a positive role in regulating cGAS-mediated innate immune responses in human and mouse cell lines. USP15 expression was increased after cGAS was activated by DNA. This positive feedback loop regulated cGAS activation and efficiently amplified the innate immune signaling. However, our data showed that neither the USP15 mRNA nor protein levels were detectably increased in response to stimulation with IFN-β (Supplementary Figure S2A, B), which was consistent with previously reported data (17). One report pointed out that USP15 activated a feedback loop through NF-κB/p65, but more evidence is needed to confirm this finding (42). Therefore, the mechanisms of USP15 induction and USP15-mediated positive feedback loop initiation through cGAS recognition of DNA remains to be further elaborated.

Mechanistically, we found that USP15, as a deubiquitinase, deubiquitylated cGAS. Interestingly, USP15 cleaved all ubiquitinated chains on cGAS, including K48 and K63 ubiquitination linkages. Although the E3 ligase for K48-linked ubiquitination of cGAS remains unknown, K48-linked ubiquitination of cGAS causes its autophagic degradation (43). USP15 reduced the K48-linked ubiquitination of cGAS. However, our data showed that USP15 did not influence the degradation of cGAS (Supplementary Figure S3C). In our recently published paper, we identified an E3 ligase, MARCH8, that promoted K63-linked ubiquitination of cGAS and inhibited cGAS activity (30). These data showed that USP15 also reduced MARCH8-mediated K63-linked ubiquitination of cGAS. However, how the cleavage of other ubiquitination linkages, including K6-, K11-, K27-, K29- and K33- linked ubiquitination, which is mediated by USP15, regulates cGAS function remains to be further studied. Given that the cGAS function was tightly regulated by various post-translational modifications (e.g. phosphorylation, acetylation or palmitoylation) (44–48), it is possible that USP15 might affect the stability of the enzymes responsible for cGAS post-translational modifications. In particular, our data showed that USP15 did not affect the stability of ENPP1, which is a cGAMP degradation enzyme (Supplementary Figure S3D). The relationship between USP15-mediated cGAS activation and other key

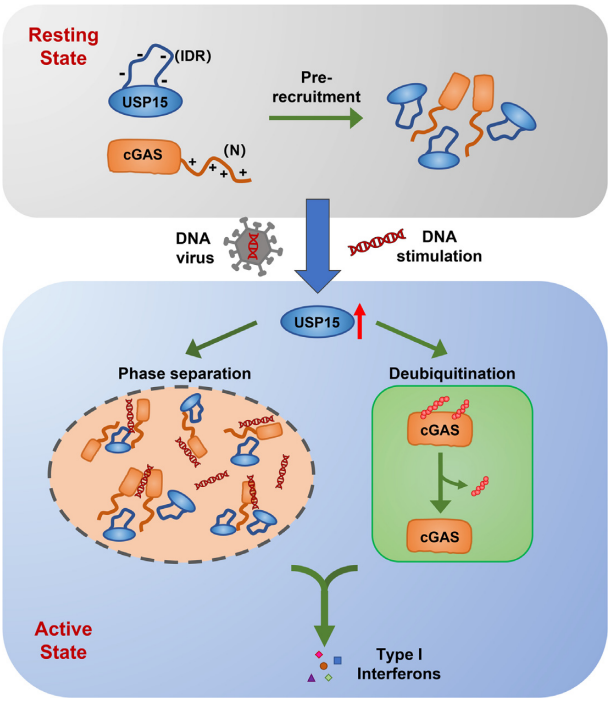

Figure 6. Proposed model for USP15-mediated cGAS activation.

players in the pathway that regulated cGAS activation remains to be elaborated in the future. Our data found that USP15 was essential for the STING signal transduction, which also requires more investigation in the future.

Moreover, we found that USP15 promoted cGAS phase separation through the USP15 IDR, which is mainly composed of negatively charged amino acids. In the absence of DNA, USP15 promoted accumulated cGAS to undergo dimerization and phase separation. Interestingly, although USP15 promoted cGAS dimerization and liquid condensation in the absence of DNA, we did not detect cGAMP production, which is essential to transduce signals that induce type I IFN expression. This outcome implies that USP15-mediated cGAS phase separation in the absence of DNA did not truly activate cGAS; however, phase separation mobilizes cGAS, enabling it to respond rapidly to DNA. Upon stimulation by dsDNA, cGAS undergoes dimerization, oligomerization and phase separation, and is activated. USP15 was induced to express and promote cGAS dimerization, oligomerization, phase separation and, importantly, cGAS activation in the presence of DNA. Although the direct interaction between cGAS and USP15 was abolished in the GST pull-down assay, their interaction remained to some extent after the IDR of USP15 was deleted in the co-IP assay, indicating the indirect interaction between cGAS and USP15 in cells, which might be responsible for the process of cGAS deubiquitylation by USP15 (Supplementary Figure S5D, E).

Considering these results, we proposed an elaborate regulatory mechanism to explain how and why USP15 regulates cGAS activation (Figure 6). In the resting state, USP15 interacts with cGAS, promoting its dimerization and phase separation through multivalent interactions. USP15 'sponges' cGAS before it accumulates to induce cGAS rapid recognition and activation upon challenging with DNA. Specifically, cGAS is silenced by USP15 'sponging', preventing aberrant cGAS activation. As soon as cGAS recognizes DNA, it oligomerizes and undergoes phase separation followed by activation. When USP15 expression was induced, cGAS was deubiquitylated and DNA–cGAS liquid condensation was increased, resulting in rapid enhancement of its activation and subsequent downstream signaling.

In summary, we identified USP15 as a cGAS-interacting protein. USP15 expression was induced by DNA-mediated cGAS activation. In human and mouse cells, USP15 promoted cGAS activation, forming a positive feedback loop. Mechanistically, USP15 deubiquitylated cGAS and promoted its activation. Moreover, USP15 promoted cGAS dimerization and liquid condensation through the USP15 IDR. In the absence of DNA, USP15 drove cGAS dimerization and liquid condensation, preparing it for rapid reaction with DNA. In response to DNA, USP15 expression was induced, which promoted cGAS dimerization, phase separation and activation. The results showed that USP15-mediated cGAS deubiquitylation and phase separation are two parallel cGAS activation pathways that are triggered by the presence of DNA. Therefore, our findings identified a previously unknown positive regulatory mechanism of cGAS activation that is mediated by USP15. This new understanding of cGAS regulation might provide targets for drug development against viral infections and autoimmune diseases.

DATA AVAILABILITY

All data associated with this study are presented in the paper or the Supplementary Data. Materials that support the findings of this study are available from the corresponding author upon request.

SUPPLEMENTARY DATA

Supplementary Data are available at NAR Online.

ACKNOWLEDGEMENTS

The authors are grateful to Professor Zhengfan Jiang for sharing the HSV-1 and VACV virus strains; to Dr Ying Zhang for helpful discussion; to Gaoge Sun and Jiaqi Liang for manuscript editing; and to Meng Han for LC-MS/MS quantification. We also thank the Center of Pharmaceutical Technology (Tsinghua University) for cGAMP quantification and data collection.

FUNDING

This work was supported by the National Natural Science Foundation of China Grant [21825702, 22137004]; Beijing Outstanding Young Scientist Program [BJJWZYJH01201910003013]; and Tsinghua University Spring Breeze Fund [2020Z99CFY036]. Funding for open access charge: National Natural Science Foundation of China [21825702].
Conflict of interest statement. None declared.

REFERENCES

1. Sun,L.J., Wu,J.X. and Chen,Z.J. (2013) Cyclic GMP–AMP synthase (cGAS) is a cytosolic DNA sensor that activates type I interferon pathway by generating a second messenger. *J. Immunol.*, **190**, 786–791.
2. Burdette,D.L., Monroe,K.M., Sotelo-Troha,K., Iwig,J.S., Eckert,B., Hyodo,M., Hayakawa,Y. and Vance,R.E. (2011) STING is a direct innate immune sensor of cyclic di-GMP. *Nature*, **478**, 515–518.
3. Gao,P., Ascano,M., Wu,Y., Barchet,W., Gaffney,B.L., Zillinger,T., Serganov,A.A., Liu,Y.Z., Jones,R.A., Hartmann,G. *et al.* (2013) Cyclic [G(2′,5′) pA(3′,5′)p] is the metazoan second messenger produced by DNA-activated cyclic GMP–AMP synthase. *Cell*, **153**, 1094–1107.
4. Shang,G., Zhang,C., Chen,Z.J., Bai,X.C. and Zhang,X. (2019) Cryo-EM structures of STING reveal its mechanism of activation by cyclic GMP–AMP. *Nature*, **567**, 389–393.
5. Zhang,C., Shang,G., Gui,X., Zhang,X., Bai,X.C. and Chen,Z.J. (2019) Structural basis of STING binding with and phosphorylation by TBK1. *Nature*, **567**, 394–398.
6. Ishikawa,H., Ma,Z. and Barber,G.N. (2009) STING regulates intracellular DNA-mediated, type I interferon-dependent innate immunity. *Nature*, **461**, 788–792.
7. Dobbs,N., Burnaevskiy,N., Chen,D.D., Gonugunta,V.K., Alto,N.M. and Yan,N. (2015) STING activation by translocation from the ER is associated with infection and autoinflammatory disease. *Cell Host Microbe*, **18**, 157–168.
8. Saitoh,T., Fujita,N., Hayashi,T., Takahara,K., Satoh,T., Lee,H., Matsunaga,K., Kageyama,S., Omori,H., Noda,T. *et al.* (2009) Atg9a controls dsDNA-driven dynamic translocation of STING and the innate immune response. *Proc. Natl Acad. Sci. USA*, **106**, 20842–20846.
9. Chen,Q., Sun,L.J. and Chen,Z.J.J. (2016) Regulation and function of the cGAS–STING pathway of cytosolic DNA sensing. *Nat. Immunol.*, **17**, 1142–1149.
10. Zhang,Q., Tang,Z., An,R., Ye,L.Y. and Zhong,B. (2020) USP29 maintains the stability of cGAS and promotes cellular antiviral responses and autoimmunity. *Cell Res.*, **30**, 821–822.
11. Chen,M.X., Meng,Q.C., Qin,Y.F., Liang,P.P., Tan,P., He,L., Zhou,Y.B., Chen,Y.J., Huang,J.J., Wang,R.F. *et al.* (2016) TRIM14 inhibits cGAS degradation mediated by selective autophagy receptor p62 to promote innate immune responses. *Mol. Cell*, **64**, 105–119.
12. Zhao,M., Xia,T., Xing,J.Q., Yin,L.H., Li,X.W., Pan,J., Liu,J.Y., Sun,L.M., Wang,M., Li,T.T. *et al.* (2022) The stress granule protein G3BP1 promotes pre-condensation of cGAS to allow rapid responses to DNA. *EMBO Rep.*, **22**, e53166.
13. Xu,G.J., Liu,C., Zhou,S., Li,Q.J., Feng,Y., Sun,P.P., Feng,H., Gao,Y.N., Zhu,J.P., Luo,X. *et al.* (2021) Viral tegument proteins restrict cGAS–DNA phase separation to mediate immune evasion. *Mol. Cell*, **81**, 2823–2837.
14. Guey,B. and Ablasser,A. (2022) Emerging dimensions of cellular cGAS–STING signaling. *Curr. Opin. Immunol.*, **74**, 164–171.
15. Lv,M.Z., Chen,M.X., Zhang,R., Zhang,W., Wang,C.G., Zhang,Y., Wei,X.M., Guan,Y.K., Liu,J.J., Feng,K.C. *et al.* (2020) Manganese is critical for antitumor immune responses via cGAS–STING and improves the efficacy of clinical immunotherapy. *Cell Res.*, **30**, 966–979.
16. Wang,C.G., Guan,Y.K., Lv,M.Z., Zhang,R., Guo,Z.Y., Wei,X.M., Du,X.X., Yang,J., Li,T., Wan,Y. *et al.* (2018) Manganese increases the sensitivity of the cGAS–STING pathway for double-stranded DNA and is required for the host defense against DNA viruses. *Immunity*, **48**, 675–687.
17. Pauli,E.K., Chan,Y.K., Davis,M.E., Gableske,S., Wang,M.K., Feister,K.F. and Gack,M.U. (2014) The ubiquitin-specific protease USP15 promotes RIG-I-mediated antiviral signaling by deubiquitylating TRIM25. *Sci. Signal*, **7**, ra3.
18. Torre,S., Polyak,M.J., Langlais,D., Fodil,N., Kennedy,J.M., Radovanovic,I., Berghout,J., Leiva-Torres,G.A., Krawczyk,C.M., Ilangumaran,S. *et al.* (2017) USP15 regulates type I interferon response and is required for pathogenesis of neuroinflammation. *Nat. Immunol.*, **18**, 54–63.
19. Chiang,C., Pauli,E.K., Biryukov,J., Feister,K.F., Meng,M., White,E.A., Münger,K., Howley,P.M., Meyers,C. and Gack,M.U. (2018) The human papillomavirus E6 oncoprotein targets USP15 and TRIM25 to suppress RIG-I-mediated innate immune signaling. *J. Virol.*, **92**, e01737-17.
20. Huang,L., Liu,H., Zhang,K., Meng,Q., Hu,L., Zhang,Y., Xiang,Z., Li,J., Yang,Y., Chen,Y. *et al.* (2020) Ubiquitin-conjugating enzyme 2S enhances viral replication by inhibiting type I IFN production through recruiting USP15 to deubiquitinate TBK1. *Cell Rep.*, **32**, 108044.
21. Zhang,H., Wang,D., Zhong,H., Luo,R., Shang,M., Liu,D., Chen,H., Fang,L. and Xiao,S. (2015) Ubiquitin-specific protease 15 negatively regulates virus-induced type I interferon signaling via catalytically-dependent and -independent mechanisms. *Sci. Rep.*, **5**, 11220.
22. Li,T., Huang,T., Du,M., Chen,X., Du,F., Ren,J. and Chen,Z.J. (2021) Phosphorylation and chromatin tethering prevent cGAS activation during mitosis. *Science*, **371**, eabc5386.
23. Du,M. and Chen,Z.J. (2018) DNA-induced liquid phase condensation of cGAS activates innate immune signaling. *Science*, **361**, 704–709.
24. Pauli,E.K., Chan,Y.K., Davis,M.E., Gableske,S., Wang,M.K., Feister,K.F. and Gack,M.U. (2014) The ubiquitin-specific protease USP15 promotes RIG-I-mediated antiviral signaling by deubiquitylating TRIM25. *Sci. Signal*, **7**, ra3.
25. Torre,S., Polyak,M.J., Langlais,D., Fodil,N., Kennedy,J.M., Radovanovic,I., Berghout,J., Leiva-Torres,G.A., Krawczyk,C.M., Ilangumaran,S. *et al.* (2017) USP15 regulates type I interferon response and is required for pathogenesis of neuroinflammation. *Nat. Immunol.*, **18**, 54–63.
26. Georges,A., Gros,P. and Fodil,N. (2021) USP15: a review of its implication in immune and inflammatory processes and tumor progression. *Genes Immun.*, **22**, 12–23.
27. Unterholzner,L. (2013) The interferon response to intracellular DNA: why so many receptors?*Immunobiology*, **218**, 1312–1321.
28. Fang,R., Jiang,Q.F., Guan,Y.K., Gao,P.F., Zhang,R., Zhao,Z. and Jiang,Z.F. (2021) Golgi apparatus-synthesized sulfated glycosaminoglycans mediate polymerization and activation of the cGAMP sensor STING. *Immunity*, **54**, 962–975.
29. Zheng,N. and Shabek,N. (2017) Ubiquitin ligases: structure, function, and regulation. *Annu. Rev. Biochem.*, **86**, 129–157.
30. Yang,X.K., Shi,C.R., Li,H.P., Shen,S.Q., Su,C.F. and Yin,H. (2022) MARCH8 attenuates cGAS-mediated innate immune responses through ubiquitylation. *Sci. Signal*, **15**, eabk3067.
31. Li,L.Y., Yin,Q., Kuss,P., Maliga,Z., Millan,J.L., Wu,H. and Mitchison,T.J. (2014) Hydrolysis of 2′ 3′-cGAMP by ENPP1 and design of nonhydrolyzable analogs. *Nat. Chem. Biol.*, **10**, 1043–1048.
32. Ablasser,A., Goldeck,M., Cavlar,T., Deimling,T., Witte,G., Rohl,I., Hopfner,K.P., Ludwig,J. and Hornung,V. (2013) cGAS produces a 2′-5′-linked cyclic dinucleotide second messenger that activates STING. *Nature*, **498**, 380–384.
33. Li,X., Shu,C., Yi,G.H., Chaton,C.T., Shelton,C.L., Diao,J.S., Zuo,X.B., Kao,C.C., Herr,A.B. and Li,P.W. (2013) Cyclic GMP–AMP synthase is activated by double-stranded DNA-induced oligomerization. *Immunity*, **39**, 1019–1031.
34. Zhang,X., Wu,J., Du,F., Xu,H., Sun,L., Chen,Z., Brautigam,C.A., Zhang,X. and Chen,Z.J. (2014) The cytosolic DNA sensor cGAS forms an oligomeric complex with DNA and undergoes switch-like conformational changes in the activation loop. *Cell Rep.*, **6**, 421–430.
35. Wang,C., Guan,Y., Lv,M., Zhang,R., Guo,Z., Wei,X., Du,X., Yang,J., Li,T., Wan,Y. *et al.* (2018) Manganese increases the sensitivity of the cGAS–STING pathway for double-stranded DNA and is required for the host defense against DNA viruses. *Immunity*, **48**, 675–687.
36. Li,X., Shu,C., Yi,G., Chaton,C.T., Shelton,C.L., Diao,J., Zuo,X., Kao,C.C., Herr,A.B. and Li,P. (2013) Cyclic GMP–AMP synthase is activated by double-stranded DNA-induced oligomerization. *Immunity*, **39**, 1019–1031.
37. Du,M.J. and Chen,Z.J.J. (2018) DNA-induced liquid phase condensation of cGAS activates innate immune signaling. *Science*, **361**, 704–709.
38. Niederkorn,M., Hueneman,K., Choi,K., Varney,M.E., Romano,L., Pujato,M.A., Greis,K.D., Inoue,J., Meetei,R. and Starczynowski,D.T. (2020) TIFAB regulates USP15-mediated p53 signaling during stressed and malignant hematopoiesis. *Cell Rep.*, **30**, 2776–2790.

39. Chen,L.L., Smith,M.D., Lv,L., Nakagawa,T., Li,Z.J., Sun,S.C., Brown,N.G., Xiong,Y. and Xu,Y.P. (2020) USP15 suppresses tumor immunity via deubiquitylation and inactivation of TET2. *Sci. Adv.*, **6**, eabc9730.
40. Lu,Y., Qiu,Y., Chen,P., Chang,H.S., Guo,L.Q., Zhang,F., Ma,L., Zhang,C., Zheng,X., Xiao,J. *et al.* (2019) ER-localized Hrd1 ubiquitinates and inactivates Usp15 to promote TLR4-induced inflammation during bacterial infection. *Nat. Microbiol.*, **4**, 2331–2346.
41. Eichhorn,P.J., Rodon,L., Gonzalez-Junca,A., Baselga,J. and Seoane,J. (2012) USP15 stabilizes the TGF-beta receptor I and promotes oncogenesis through the activation of the TGF-beta signal in glioblastoma. *Cancer Res.*, **72**, 429–435.
42. Zhou,L., Jiang,H., Du,J., Li,L., Li,R., Lu,J., Fu,W. and Hou,J. (2018) USP15 inhibits multiple myeloma cell apoptosis through activating a feedback loop with the transcription factor NF-κBp65. *Exp. Mol. Med.*, **50**, 1–12.
43. Chen,M., Meng,Q., Qin,Y., Liang,P., Tan,P., He,L., Zhou,Y., Chen,Y., Huang,J., Wang,R.F. *et al.* (2016) TRIM14 inhibits cGAS degradation mediated by selective autophagy receptor p62 to promote innate immune responses. *Mol. Cell*, **64**, 105–119.
44. Dai,J., Huang,Y.J., He,X.H., Zhao,M., Wang,X.Z., Liu,Z.S., Xue,W., Cai,H., Zhan,X.Y., Huang,S.Y. *et al.* (2019) Acetylation blocks cGAS activity and inhibits self-DNA-induced autoimmunity. *Cell*, **176**, 1447–1460.
45. Li,T., Huang,T.Z., Du,M.J., Chen,X., Du,F.H., Ren,J.Y. and Chen,Z.J. (2021) Phosphorylation and chromatin tethering prevent cGAS activation during mitosis. *Science*, **371**, eabc5386.
46. Shi,C.R., Yang,X.K., Liu,Y., Li,H.P., Chu,H.Y., Li,G.H. and Yin,H. (2022) ZDHHC18 negatively regulates cGAS-mediated innate immunity through palmitoylation. *EMBO J.*, **41**, e109272.
47. Song,B.K., Greco,T.M., Lum,K.K., Taber,C.E. and Cristea,I.M. (2020) The DNA sensor cGAS is decorated by acetylation and phosphorylation modifications in the context of immune signaling. *Mol. Cell. Proteomics*, **19**, 1193–1208.
48. Zhong,L., Hu,M.M., Bian,L.J., Liu,Y., Chen,Q. and Shu,H.B. (2020) Phosphorylation of cGAS by CDK1 impairs self-DNA sensing in mitosis. *Cell Discov*, **6**, 26.